Evaluation of Variable-Depth Liner Configurations for Increased Broadband Noise Reduction

M. G. Jones*, W. R. Watson†, D. M. Nark‡, and B. M. Howerton§
NASA Langley Research Center, Hampton, VA 23681

This paper explores the effects of variable-depth geometry on the amount of noise reduction that can be achieved with acoustic liners. Results for two variable-depth liners tested in the NASA Langley Grazing Flow Impedance Tube demonstrate significant broadband noise reduction. An impedance prediction model is combined with two propagation codes to predict corresponding sound pressure level profiles over the length of the Grazing Flow Impedance Tube. The comparison of measured and predicted sound pressure level profiles is sufficiently favorable to support use of these tools for investigation of a number of proposed variable-depth liner configurations. Predicted sound pressure level profiles for these proposed configurations reveal a number of interesting features. Liner orientation clearly affects the sound pressure level profile over the length of the liner, but the effect on the total attenuation is less pronounced. The axial extent of attenuation at an individual frequency continues well beyond the location where the liner depth is optimally tuned to the quarter-wavelength of that frequency. The sound pressure level profile is significantly affected by the way in which variable-depth segments are distributed over the length of the liner. Given the broadband noise reduction capability for these liner configurations, further development of impedance prediction models and propagation codes specifically tuned for this application is warranted.

I. Introduction

Commercial air traffic continues to increase, causing additional noise exposure for communities surrounding airports. In an attempt to alleviate this concern, the Federal Aviation Administration (FAA) and International Civil Aviation Organization (ICAO) have imposed increasingly stringent aircraft noise requirements. In response to these requirements, one of the key components of the National Aeronautics and Space Administration (NASA) Advanced Air Vehicle Program is to develop innovative aircraft noise reduction concepts. One approach to engine fan noise reduction is the incorporation of acoustic liners in the interior walls of the aircraft engine nacelle.

The bypass ratio of commercial aircraft engines has steadily increased over the last few decades. This has resulted in a transition in the character of the fan noise spectrum, from one dominated by tones (e.g., at multiples of the blade passage frequency) to a broadband spectrum overlaid with less dominant tones. In response to this evolution of the fan noise spectrum, conventional acoustic liners have transitioned from single-layer, perforate-over-honeycomb configurations to double-layer configurations with embedded porous septa that are more suitable for broadband fan noise reduction. However, there remains a need for further broadband noise reduction, to include (1) an extension of the frequency range for which noise reduction occurs, and (2) an increase in the amount of noise reduction achieved over this frequency range. Variable-depth liners (liner depth varies over its axial and/or circumferential extent) offer potential for achieving this increased broadband noise reduction. One such configuration, in which the depth is linearly varied over the length of the liner, was demonstrated to provide significant sound absorption over a broad frequency range.[1]

*Senior Research Scientist, Research Directorate, Structural Acoustics Branch, AIAA Associate Fellow.
†Senior Research Scientist, Research Directorate, Computational AeroSciences Branch, AIAA Associate Fellow.
‡Senior Research Scientist, Research Directorate, Structural Acoustics Branch, AIAA Associate Fellow.
§Research Scientist, Research Directorate, Structural Acoustics Branch, AIAA Senior Member.

The three-fold purpose of the current study is (1) to validate an impedance prediction model for variable-depth liners with and without grazing flow, (2) to evaluate the broadband absorptive properties of these liners, and (3) to develop improved variable-depth liner configurations (e.g., lighter, thinner, and more absorptive). In the earlier study,[1] a transmission line model was successfully used to predict the surface impedance variability over the axial extent of the variable-depth liner. However, this model did not include the effects of grazing flow over the liner. In the current study, a different model[2,3] is employed that allows for inclusion of mean flow effects. This model is used with two duct acoustics propagation codes[4,5] based on the convected Helmholtz equation to predict sound pressure level, SPL, axial profiles for a variable-depth liner mounted in the NASA LaRC Grazing Flow Impedance Tube (GFIT). These predicted axial profiles are compared with data measured in the GFIT for validation of the impedance prediction model. The predicted (and measured) sound pressure level axial profiles are then used to gain insight into the sound absorption mechanisms. Finally, one of these propagation codes is used to explore multiple variable-depth configurations that use these absorption mechanisms to optimize broadband noise reduction.

Section II provides a description of the experimental methods used to evaluate the liner configurations, and also provides a description of each of the test liners used in this study. The impedance prediction model is presented in Section III, and the acoustic propagation models are briefly described in Section IV. Results are discussed in Section V, and the primary conclusions of the study are presented in Section VI.

II. Experimental Method

A. Grazing Flow Impedance Tube (GFIT)

The GFIT has a cross-sectional geometry of 50.8 mm wide by 63.5 mm high, and allows evaluation of acoustic liners with lengths from 50.8 mm to 609.6 mm. The surface of the test liner forms a portion of the upper wall of the flow duct. For the current investigation, the source section consists of twelve acoustic drivers mounted upstream (exhaust mode) of the test section. (Fig. 1 shows an earlier configuration with eighteen drivers.) For this study, these drivers were used to generate tones (one frequency at a time) at 130 dB over a frequency range of 400 to 3000 Hz. These tests were conducted at GFIT centerline Mach numbers of 0.0, 0.3, and 0.5.

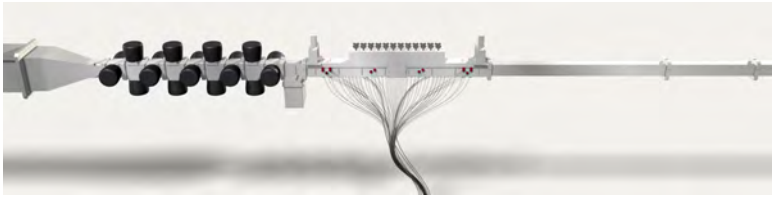

Figure 1: Sketch of Grazing Flow Impedance Tube (GFIT).

Fifty-three microphones flush-mounted in the wall opposite the liner (i.e., the lower wall) are used to measure the acoustic pressure field over the axial extent of $0 \leq x \leq L$ (see Fig. 2). For each data acquisition, 1000 averages on each microphone channel (1024 data points per average) are taken. A cross-spectrum signal extraction method[6] is used to determine the amplitudes and phases at each of the microphone locations relative to the amplitude and phase at the reference microphone location upstream of the lined section.

B. Test Liners

Two 406.4 mm-long liners (see Fig. 3) were fabricated using a 3-D printing, stereolithography (SLA) process for evaluation in the GFIT. The perforate facesheet and core chambers were fabricated as a single piece for each of these liners. The back plates for these liners were fabricated separately, and the two components (facesheet/core and back plate) are press fit together to form the full test liner. The facesheet for each

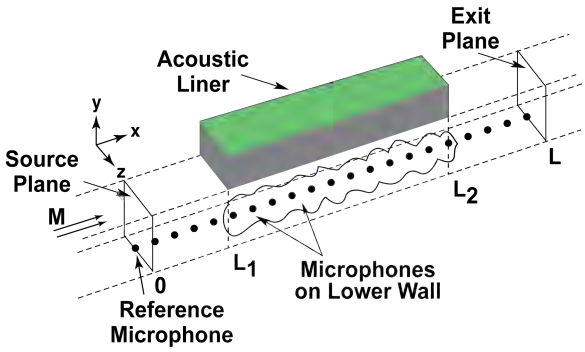

Figure 2: Sketch of Grazing Flow Impedance Tube test section.

liner has a porosity of 5.5%, a thickness of 0.8 mm, and an orifice diameter of 1.0 mm. These dimensions were chosen such that the liners would provide significant attenuation for the Mach 0.0 condition. The first liner (TL1) has a core depth that varies linearly from 15.2 to 74.6 mm over the full 406.4 mm length. The second liner (TL2) has two 203.2 mm-long zones. The core depth varies linearly from 46.7 to 76.2 mm over the first zone, and is constant at 76.2 mm over the second zone. For both liners, the core chambers are 15.2 mm $\times$ 15.2 mm, and are separated by 2.5 mm-wide partitions. There are 22 core chambers in the axial dimension, and 3 core chambers in the spanwise dimension, for a total of 66 core chambers in each liner. Each of these liners were tested in two orientations. In the following discussion, 'U' or 'D' labels are added when the maximum depth is at the upstream (e.g., TL1U) or downstream (e.g., TL1D) ends of the liner, respectively.

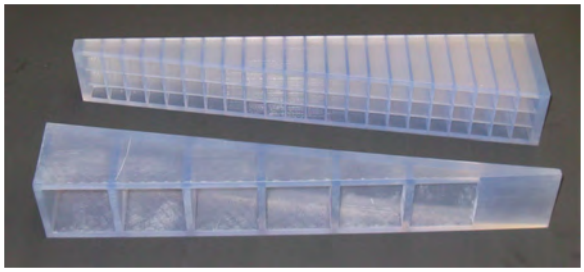

(a) Variable-depth liner with back plate (TL1).

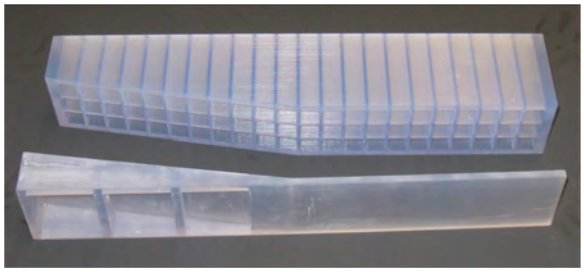

(b) Two-zone, variable-depth liner with back plate (TL2).

Figure 3: Photographs of variable-depth perforate-over-honeycomb liners constructed via an SLA process.

III. Impedance Prediction Model

The semi-empirical Two-Parameter (TP) model[2,3] is used to predict the single-layer, perforate-over-honeycomb liner acoustic impedance

$$\zeta = \theta + i\chi \tag{1}$$

where θ and χ are the normalized resistance and reactance components of the normalized acoustic impedance, ζ. The TP model assumes the thickness of the perforate facesheet is sufficiently small, relative to the shortest acoustic wavelength of interest, to be treated as a lumped element. The normalized resistance, θ, is based on an analytic structure inferred from the one-dimensional momentum equation,[7] and is given by

$$\theta = \frac{a\mu t}{2\rho c(\sigma C_D)d^2} + \frac{k_i + k_e}{2c(\sigma C_D)^2} V_{rms} + \theta_{\text{gf}} \tag{2}$$

where t, d, and σ are the facesheet thickness, hole diameter, and surface open area ratio, respectively. The RMS acoustic particle velocity is denoted as V_{rms}, and μ, ρ and c are the viscosity, density and sound speed, respectively. The empirical constants k_i and k_e account for entrance and exit end effects of the facesheet holes, and their sum is taken to have the value of unity. The discharge coefficient, C_D, accounts for vorticity-related losses at the hole exit, and is generally set to a value of 0.76 for sharp-edged holes. In this derivation, the first term on the right can be found in Darcy's law[8] for seepage flow through porous media and the second term on the right can be found in orifice metering theory.[9] For laminar flow in circular orifices, a is assigned[8] a value of 32. The last term accounts for grazing flow, e.g., through the aircraft engine nacelle. The value for this term is estimated using the classical Rice-Heidelberg model[10] given by

$$\theta_{gf} = \frac{M_{ave}}{\left(2 + 1.256\frac{\delta^*}{d}\right)\sigma} \tag{3}$$

where θ_{gf} is the normalized grazing flow resistance, δ^* is the boundary layer displacement thickness, and M_{ave} is the free-stream, average Mach number. Clearly, this term will become dominant at high mean flow velocities.

The normalized reactance is given by

$$\chi = -cot(kh) + \frac{k(t + \epsilon d)}{\sigma C_D} \tag{4}$$

where h is the honeycomb core height (cavity depth), k is the freespace wavenumber, and the hole length end correction, ϵd, is computed via

$$\epsilon = \frac{0.85(1 - 0.7\sqrt{\sigma})}{1 + 305M_{ave}^3} \tag{5}$$

The second term of equation 4 is the normalized mass reactance due to the perforate facesheet. The total normalized acoustic impedance, ζ, is given by the combination of equations 2 and 4.

IV. Acoustic Propagation Codes

Two acoustic propagation codes, labeled as CHE and CDL, are used in this study. Each of these codes has been described in detail in earlier publications.[11,12] Thus, for the sake of brevity, the following discussion is limited to a description of those features that are of particular importance to the current investigation. Both codes assume the liner to be installed on the upper wall (as in the GFIT, see Fig. 2) and allow the impedance to vary along the axial length of the liner. For the current study, both codes assume a uniform mean flow and the liner impedance is assumed constant in the cross dimension.

The CHE propagation code[11] uses a finite element model of the convected Helmholtz equation. This model includes the effects of reflections at the leading (LE) and trailing (TE) edges of the liner, and also allows for inclusion of the effects of reflections at the termination. The CDL propagation code[12] utilizes a parabolic approximation to the convected Helmholtz equation and is a computationally efficient model that accounts for fully three-dimensional geometries. The parabolic approximation neglects reflections due to impedance discontinuities at the leading ($x = L_1$) and trailing ($x = L_2$) edges of the liner (see Fig. 2), as well as at the termination ($x = L$).

V. Results and Discussion

A number of different types of results are provided herein. First, SPL profiles acquired in the GFIT with two variable-depth liners, TL1 and TL2, are discussed. These data clearly demonstrate the potential for usage of variable-depth liners to achieve broadband noise reduction. Next, impedances predicted for the individual cells of these liners are used as input to a propagation code to predict the corresponding SPL profiles. A comparison between the measured and predicted SPL profiles is used to evaluate the ability to use this approach to study variable-depth liners. This comparison is quite favorable over the full range of test conditions, but some difficulties are observed in the frequency range of interest, which corresponds to the

frequency range of maximum attenuation. Nevertheless, there are sufficient similarities to lend confidence that the impedance prediction model and propagation code can be confidently used for exploration of the effects of varying the liner geometry. With this in mind, a number of variable-depth liner configurations are assessed, and their respective SPL profiles are used to explore interesting features of variable-depth liners.

A. Measured SPL Profiles

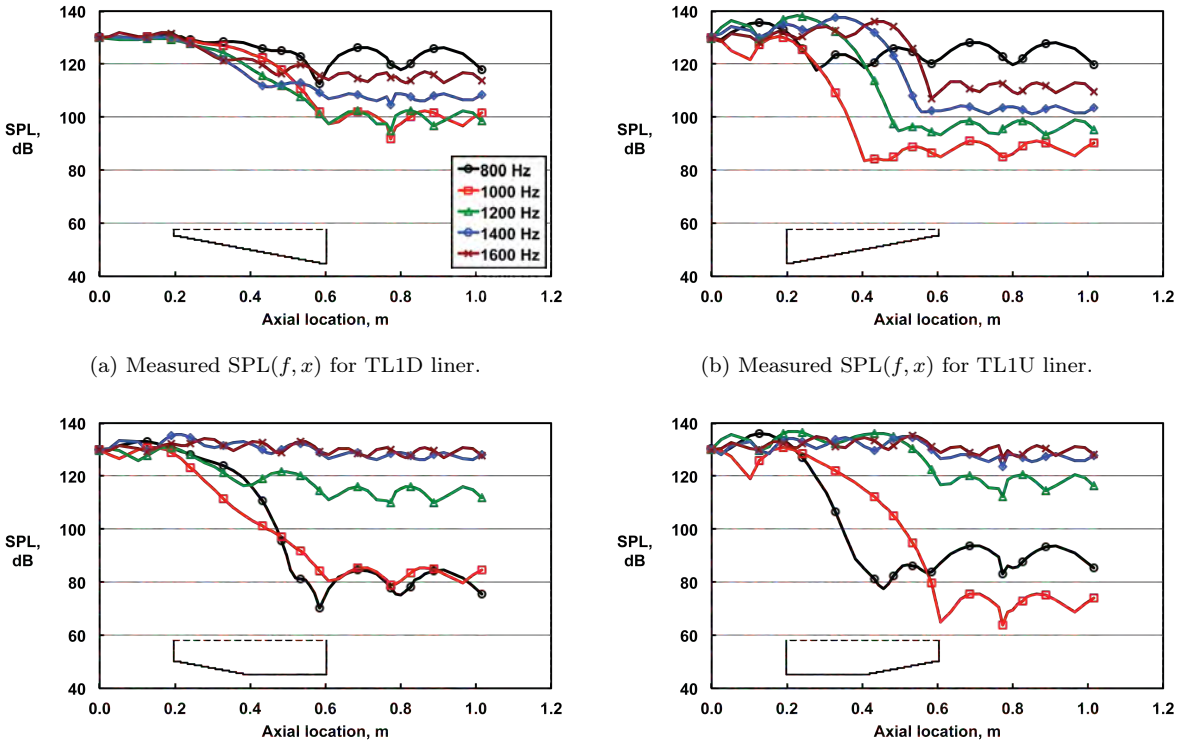

(a) Measured SPL(f, x) for TL1D liner.

(b) Measured SPL(f, x) for TL1U liner.

(c) Measured SPL(f, x) for TL2D liner.

(d) Measured SPL(f, x) for TL2U liner.

Figure 4: Effects of liner geometry on axial pressure profile, SPL(f, x); Mach 0.0.

The main focus of the current research is to explore the effects of axially varying the acoustic impedance of a liner mounted in the wall of a flow duct. Figure 4 provides sound pressure level profiles [SPL(f, x)] acquired in the GFIT with the two variable-depth, test liners described in Section II.B. Each graph contains a sketch of the liner that was tested, along with its orientation. The liner extends over the range of $x \in (0.2, 0.6)$ m, and the mean flow and acoustic source are generated upstream of the liner ($x < 0.0$ m). As indicated in Section II.A, tests were conducted over the frequency range of 400 to 3000 Hz. However, the results presented in the current report will generally be limited to the frequency range of 800 to 1600 Hz, as this is the frequency range for which the greatest attenuations occur. It is noted that this choice of frequency range will certainly influence the interpretation of results to follow.

Significant attenuation is observed for frequencies over a range of at least one octave. Separate tests with a constant-depth liner constructed in a similar manner show somewhat greater attenuation at a single frequency, but much less attenuation at the remaining frequencies. It is also interesting to note that this increased bandwidth is achieved by the elimination of liner material (i.e., reduced depth over a portion of the liner). Given the continued need for broadband noise reduction, this suggests that the trade-off of liner complexity for increased broadband noise reduction may be worth pursuing. Clearly, liner orientation has a significant effect for this frequency range. The amount of attenuation is larger for the TL1U liner over the frequency range for which the liner is optimized ($\geq$1000 Hz). Also, Fig. 4-a shows that attenuation occurs over the full extent of the TL1D liner, whereas the axial extent of the attenuation (the portion of the curve where the SPL continues to decrease) is reduced when the liner orientation is reversed (TL1U,

see Fig. 4-b). There are distinct liner orientation effects for the TL2 liner as well. Although the effects are clearly frequency-dependent, the maximum attenuation (at 1000 Hz) is again achieved when the maximum depth is at the upstream end of the liner.

B. Comparison of Measured and Predicted SPL Profiles

One goal of the current study was to evaluate the current impedance prediction model for variable-depth liners with and without grazing flow. The impedance prediction model (see Section III) was used to predict the impedance distribution, $\zeta(f, x)$, over the length of the liner. This impedance distribution was then used as input for the CHE propagation code to predict the SPL profile over the length of the liner. Comparison of these predicted profiles with data measured in the GFIT (for Mach numbers of 0.0, 0.3, and 0.5) was used to evaluate this process. The CHE was used for this evaluation because it supports inclusion of the measured exit impedance, ζ_{exit}, boundary condition.

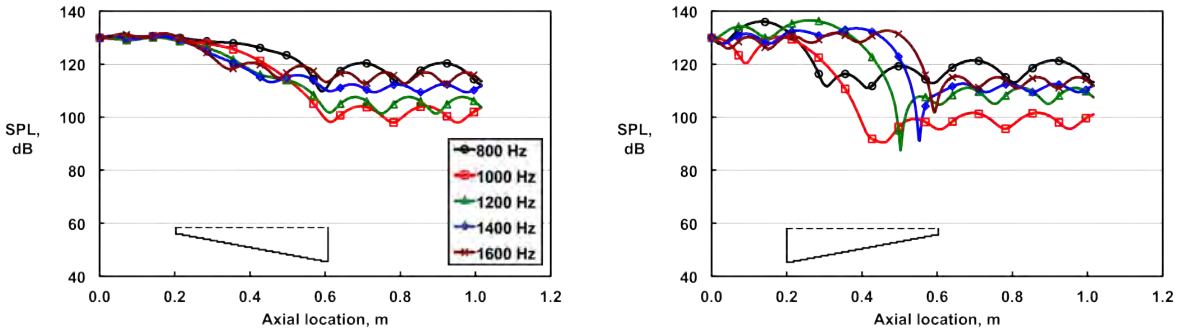

(a) Predicted SPL(f, x) for TL1D liner.

(b) Predicted SPL(f, x) for TL1U liner.

Figure 5: Effects of geometry on axial pressure profiles, SPL(f, x), predicted with CHE code using ζ_{exit} termination; Mach 0.0.

Figures 4 (parts 'a' and 'b') and 5 provide comparisons of measured and predicted sound pressure level profiles as a function of frequency and axial location (distance from source plane; $x = 0$ in Fig. 2), SPL(f, x), for the TL1 test liner (forward and reverse configurations), and for the $M = 0.0$ condition. In general, the comparison between predicted and measured results for the TL1D liner is quite favorable, although there is slightly more spread among the measured profiles. When the liner orientation is reversed (TL1U), this feature is accentuated, i.e., the spread among the measured profiles grows to about 10 dB more than is observed in the spread among the predicted profiles. Overall, the predicted profiles tend to be conservative, i.e., predict less attenuation than is measured. In general, it should be noted that the poorest comparison occurs for this frequency range of maximum attenuation and for the no-flow condition. The comparison improves for frequencies away from this sensitive region, and it improves across the entire frequency range as the mean flow is engaged. In fact, when the entirety of the dataset (measured and predicted results, four liner configurations, three Mach numbers, 14 frequencies) is considered, this comparison is quite favorable.

The measured and predicted SPL profiles are quite sensitive at test conditions for which significant attenuation occurs, i.e., small changes in frequency can result in significant changes in attenuation. Therefore, one possible topic for further evaluation is the application of the impedance prediction model used in this study. This impedance prediction model (and other similar models) has been successfully used for decades to predict the acoustic impedance for conventional, constant-depth, perforate-over-honeycomb liners. For the current study, this model is used to predict the impedance of each individual cell, and this axial distribution of impedances is used as input in the propagation code. Although this seems to be a reasonable extension in the usage of the model, there are some possible issues to be considered. For example, the wavelength of the impinging tone for the frequency range considered in this study is significantly longer than the diameter of the individual cell. Hence, the effects of adjacent cells, each with a unique impedance, are in some sense

averaged (smeared) beyond the confines of the individual cell. The current model does not account for interactive effects between adjacent cells at the surface of the liner.

Propagation codes have been used for decades[13] to predict the effects of axially varying surface impedance (i.e., axially segmented liners) on the sound pressure level profiles over the length of the liner. However, the impedance variability does not typically occur on such a small axial scale (i.e., a discrete change in impedance occurs every 18 mm). There is an impedance discontinuity at the interface between two adjacent axial cells, which the CHE propagation code models using a weak formulation. As indicated above, this approach works fine over the majority of the frequency and Mach number regimes considered in this study, but is less robust at test conditions for which large attenuations are observed. Given the additional issues brought about by the current application of interest, further evaluation of these implementations of the impedance prediction model and the propagation code are warranted, and are expected to be the focus of future investigations. Regardless, the measured and predicted trends are sufficiently similar to indicate the current modeling approach is suitable for evaluation of proposed variable-depth liner configurations.

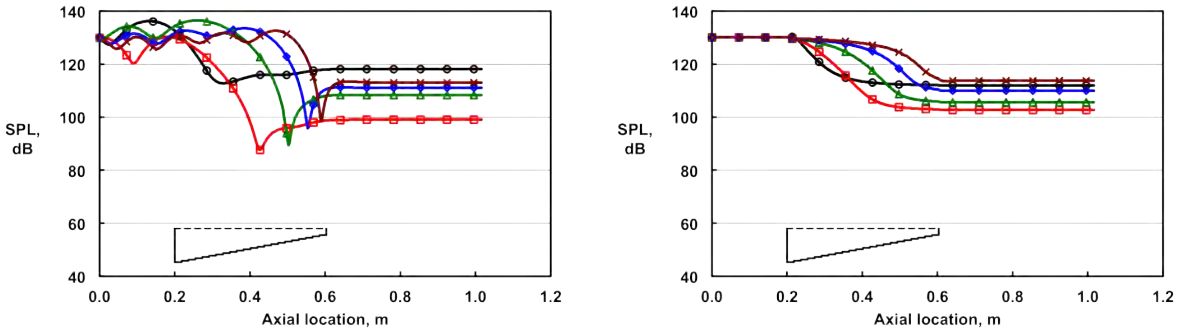

(a) Predicted SPL(f, x); CHE, ρc termination.

(b) Predicted SPL(f, x); CDL.

Figure 6: Predicted SPL(f, x) for TL1U liner; Mach 0.0.

Figure 6 provides a comparison of sound pressure level profiles predicted with the CHE and CDL propagation codes. Since the CDL code assumes an anechoic (ρc) termination, a similar exit boundary condition is also applied for the CHE. As expected, the profiles predicted with both codes have zero slope in the hard wall section downstream of the liner. As the CDL code is based on a parabolic approximation to the convected Helmholtz equation, it does not support reflections. This is evidenced by the lack of standing wave patterns upstream of the liner LE and TE. Overall, the CDL predicted attenuations are observed to be more clustered (less frequency dependence), but the frequency-dependence of the attenuation is the same for both codes.

C. Grazing Flow Effects

Figure 7 provides a comparison of measured and predicted sound pressure level profiles for the TL1U liner, with a grazing flow Mach number of 0.3. Comparison of Figures 4-b and 7-a shows that mean flow causes the attenuation to be significantly reduced. Interestingly, it also causes the axial extent over which the attenuation occurs to be lengthened. For example, the SPL profile for the 1000 Hz condition reaches a minimum at $x \simeq 0.4$ m for the no-flow condition (Fig. 4), but does not reach a minimum until $x \simeq 0.5$ m for the Mach 0.3 condition. This same feature is also observed in the results predicted with the CHE for Mach 0.0 (Fig. 5-b) and Mach 0.3 (Fig. 7-b). Regardless, the comparison is quite favorable.

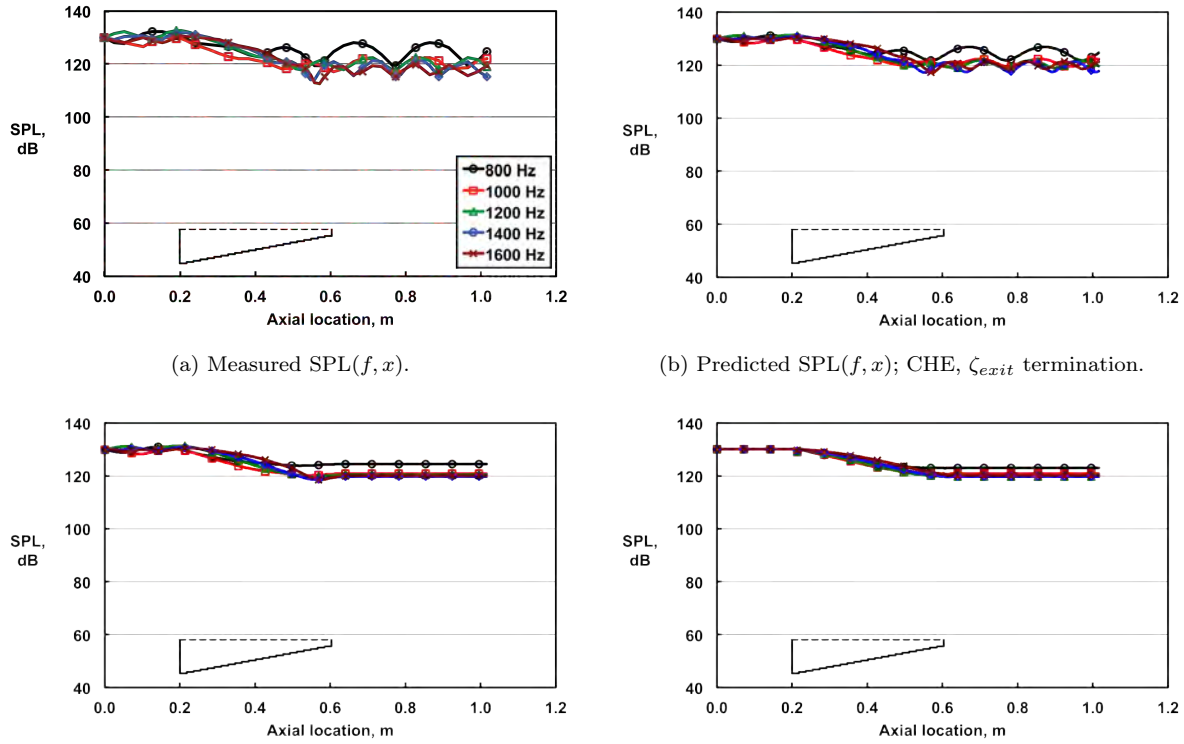

(a) Measured SPL(f, x).

(b) Predicted SPL(f, x); CHE, ζ_{exit} termination.

(c) Predicted SPL(f, x); CHE, ρc termination.

(d) Predicted SPL(f, x); CDL.

Figure 7: Comparison of measured and predicted SPL(f, x) for TL1U liner; Mach 0.3.

As observed earlier, the effects of switching from a measured exit impedance boundary condition, ζ_{exit}, to an anechoic (ρc) exit boundary condition for the CHE predictions are as expected. When the measured exit impedance is used, the standing waves in the downstream hard wall section are captured. If the anechoic termination is employed, the SPL profiles flatten out in the hard wall section downstream of the liner. As noted earlier, the CDL code does not capture the standing waves just upstream of the leading and trailing edges of the liner. Nevertheless, the comparison between the CHE and CDL results is quite favorable.

Overall, at least for this frequency range of maximum attenuation, both codes provide good estimates of the measured SPL profiles, and are therefore believed to be suitable for evaluation of variable-depth liner geometry.

D. Liner Geometry Effects

For the final portion of the study, the CHE code was used with the impedance prediction model to evaluate the effects of liner geometry on the frequency-dependent noise reduction. These simulations were based on the GFIT geometry, with an anechoic exit boundary condition. The GFIT geometry was selected such that those liner configurations that produced notable acoustic performance could be fabricated and tested at a later date. Only 2D liner configurations (no impedance variability in the span-wise dimension) were considered for simplicity and to minimize computational requirements. Thus, either of the propagation codes would be suitable for this optimization. The CHE code was chosen because the liners of interest employ a facesheet that causes the optimum attenuation to occur at Mach 0.0, and the CHE was demonstrated earlier to provide the best results for this test condition. The choice of the exit boundary condition was not as clear cut. If the measured exit impedance was used, this would be expected to give the best comparison with measured data. However, the liner designer is not typically provided the exit impedance. Thus, given the fact that the earlier predicted results showed that the two exit boundary conditions provided very similar results, the anechoic termination was chosen for this study. Each of the simulated liners is assumed to be

constructed similar to the TL1 liner described in Section II.B, i.e., to consist of twenty-two axial segments, each of which can be any depth between 15.2 and 74.6 mm.

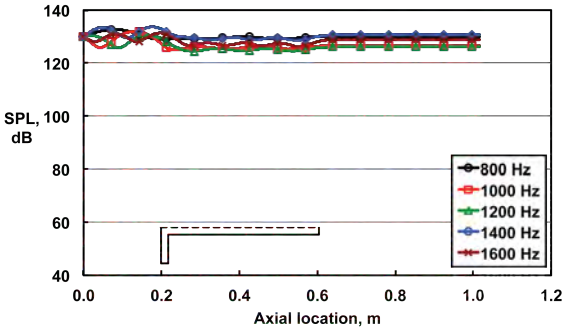

(a) Configuration L1.

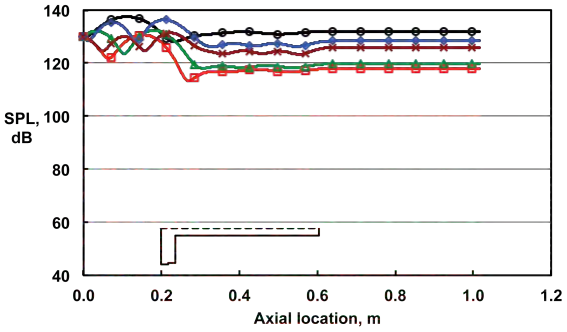

(b) Configuration L2.

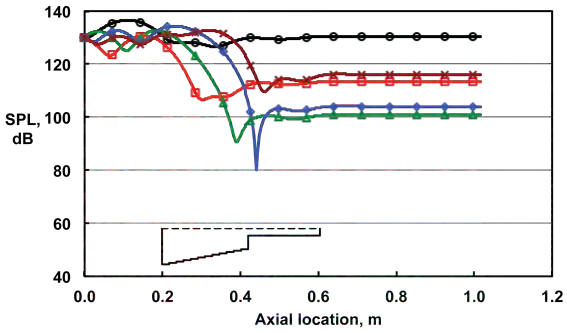

(c) Configuration L3.

Figure 8: Comparison of liner geometries on bandwidth of liner attenuation; CHE code, Mach 0.0.

Figure 8 provides the predicted SPL profiles for three liner configurations, labeled L1 - L3, with geometries based on the TL1U liner. The first (L1) has one segment that is 74.6 mm deep (same as TL1U), but the remainder (23 segments) are 15.2 mm deep. The second (L2) uses the first two segments of the TL1U liner, with the remainder at 15.2 mm deep. The third (L3) uses the first eleven segments of the TL1U liner, with the remainder at 15.2 mm deep. A comparison of these three configurations provides some interesting features. For the L1 configuration, there is a minimal amount of attenuation at 1000 and 1200 Hz, the frequencies nearest resonance for the first segment. The frequencies that would be best attenuated by this liner (i.e., frequencies with quarter-wavelengths close to 15.2 mm) are well above the frequency range considered in this study (400 to 3000 Hz). When the additional deep segment is added (L2), the attenuation at 1000 and 1200 Hz increases and the bandwidth also increases (increased attenuation at 1400 and 1600 Hz). Also, the attenuation for these frequencies is observed to extend beyond the axial location where the deeper, 'tuned' segments occur. Although not shown in the figures, this effect is observed to continue as additional segments from the TL1U liner are incorporated into the liner configuration. When the entire first half of the TL1U liner is used (with the remainder set to a depth of 15.2 mm; L3), a significant attenuation increase is observed over all frequencies from 1000 to 1600 Hz (this observation extends to higher frequencies, but is not shown in these figures).

Comparison of the results for the L1, L2, and L3 configurations also shows that attenuation of a selected frequency is initiated at or near the axial location corresponding to where the segment depth is equal to the quarter-wavelength of that frequency. Also, the axial extent of the attenuation at an individual frequency continues well beyond the location where the quarter-wavelength is optimally tuned for that frequency. Taken together, this might suggest that variable-depth liner configurations should be designed such that

the segments near the upstream end of the liner are tuned to those frequencies for which the greatest attenuation is needed. However, the results provided in Fig. 5 demonstrated that this is not necessarily the case. Predicted results for the TL1U and TL1D liner configurations indicate that, although the SPL profiles are quite different for the two configurations, the total amount of attenuation at each frequency is relatively unchanged.

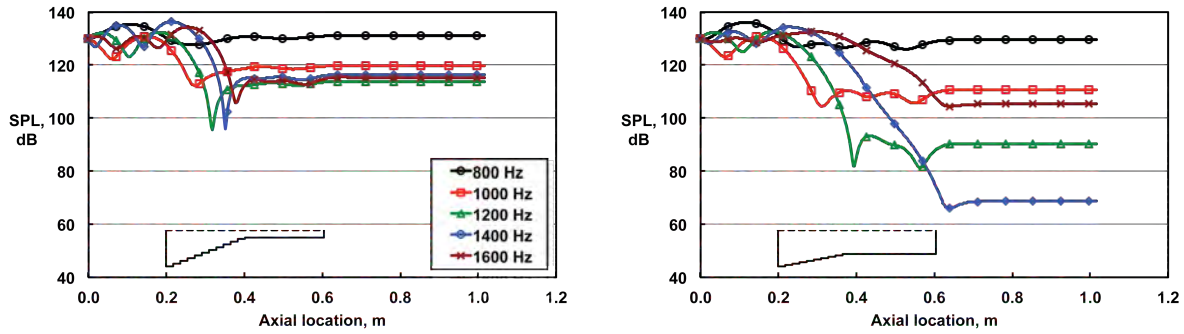

(a) Configuration L4.

(b) Configuration L5.

Figure 9: Effects of hybrid configurations (half variable-depth, half constant-depth); CHE code, Mach 0.0.

Figure 9 provides predicted results for two additional liner configurations. The L4 configuration is very similar to the L3 configuration (Fig. 8-c), except the slope of the segment depths is increased such that the step is eliminated at the axial midpoint. As might be expected, this causes the predicted attenuation to be decreased at the dominant frequencies, as the axial extent of segments with depths at or near the quarter-wavelengths of these frequencies is reduced.

The first half of the L5 geometry is identical to the L3 geometry, but the constant-depth portion is increased to 46 mm to eliminate the step that is present in the L3 geometry. The results for the L5 configuration are generally much better than those observed for the L3 geometry. Also, it is interesting to note the nature of the SPL profiles. At 1000 Hz, the attenuation rate is quite good over the first third of the liner, and then the SPL settles out to a constant value. At 1200 Hz, the attenuation is initiated a little farther from the LE of the liner, but the region of maximum attenuation extends nominally the same distance as seen for at 1000 Hz. The profiles for 1400 and 1600 Hz have a slightly different nature. Attenuation at each of these frequencies 'begins' in an orderly manner (i.e., 1600 Hz begins downstream of 1400 Hz), similar to that seen for the lower frequencies. However, the SPL profiles for these two frequencies are attenuated over a longer axial extent, with each of them continuing the attenuation over the full length of the liner.

Figures 10 and 11 provide comparisons of four different liner configurations constructed with the same group of segments, at grazing flow Mach numbers of 0.0 and 0.5 (the minimum and maximum flow conditions used in this study). The first configuration (L6) places the maximum-depth segments at the LE and TE of the liner, with the minimum-depth segments at the axial midpoint of the liner. The second configuration (L7) is the same as liner L6 over the first half, and this pattern is replicated for the second half of the liner. The third configuration (L8) places the minimum-depth segments at the LE and TE of the liner, with the maximum depth at the axial midpoint (essentially, the reverse of L6). The first half of the last configuration (L9) is identical to those of liners L6 and L7, and the depths of the segments that make up the second half of the liner are randomly distributed.

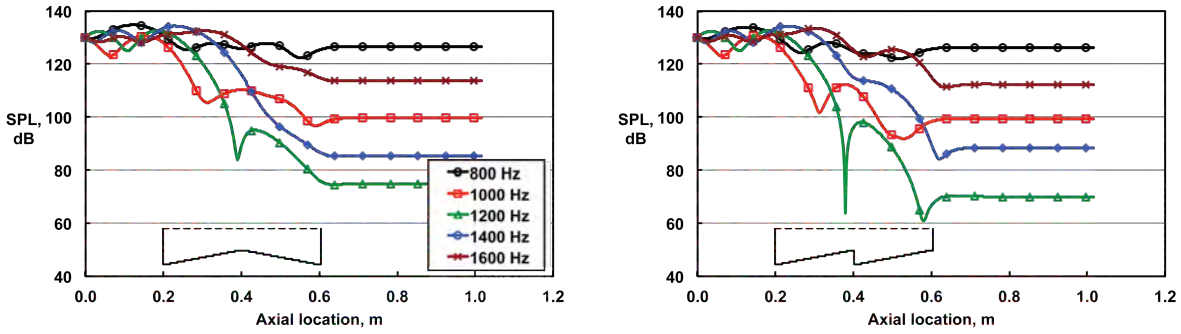

(a) Configuration L6.

(b) Configuration L7.

(c) Configuration L8.

(d) Configuration L9.

Figure 10: Effects of variable-depth segment distribution; CHE code, Mach 0.0.

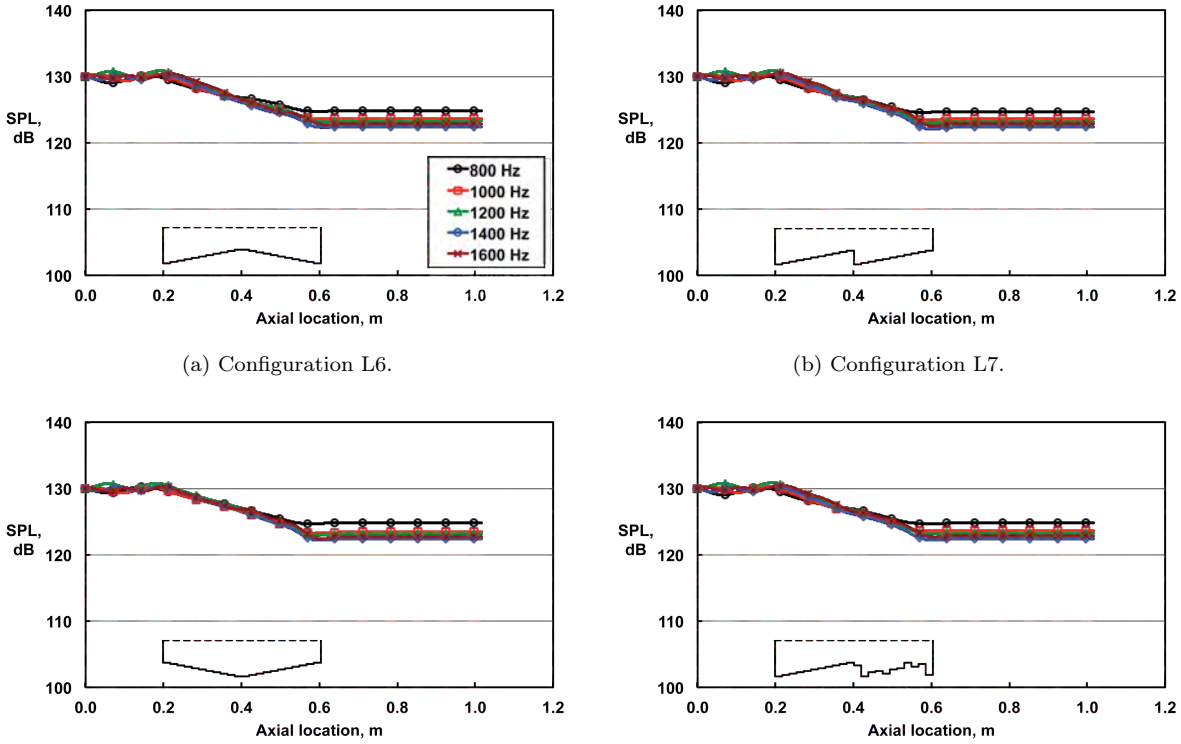

(a) Configuration L6.

(b) Configuration L7.

(c) Configuration L8.

(d) Configuration L9.

Figure 11: Effects of variable-depth segment distribution; CHE code, Mach 0.5.

In spite of the significant variability in how the variable-depth segments are distributed in these four liner configurations, the total attenuation is relatively unaffected over the frequency range of interest. However, the SPL profiles are markedly different for the different configurations. For three of the configurations (L6, L7, and L9), there is a distinct reflection at the axial midpoint of the liner at 1200 Hz, whereas this does not occur for the L8 configuration. It is expected that there is a frequency near 1200 Hz where a similar reflection would occur for the L8 configuration, but the frequency resolution (200 Hz increment) used in the analysis was insufficient to capture it. One item that is very clear is that the inclusion of mean flow tends to collapse the SPL profiles together. The maximum attenuation still occurs over the same frequency range (i.e., more attenuation for 1000 to 1600 Hz than for the remainder of the frequency range included in the study), but the amount of attenuation is significantly reduced. Of course, this is at least partially due to the choices employed in the design of the facesheet (assumed constant throughout this study), as these geometric parameters were chosen to accentuate the effects at Mach 0.0.

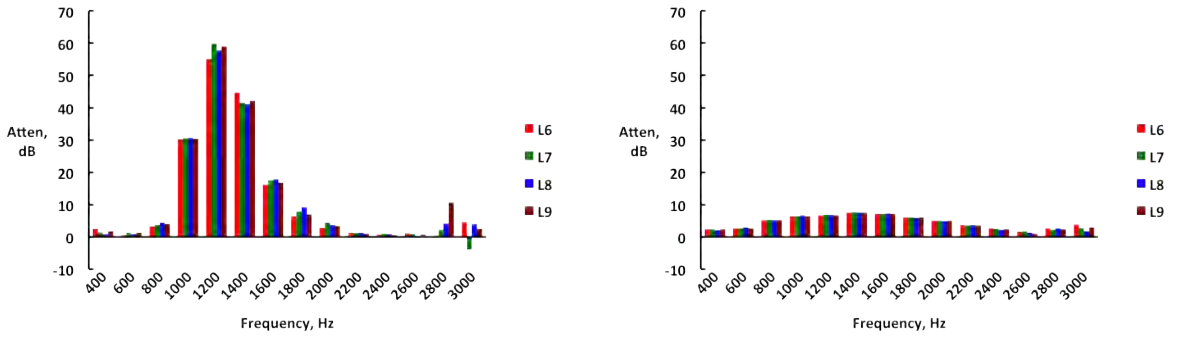

(a) Mach 0.0.

(b) Mach 0.5.

Figure 12: Attenuation [SPL(0) − SPL(L)] for liner configurations L6 - L9.

Finally, Figure 12 provides a summary of the attenuation spectra predicted for the four liner configurations presented in Figs. 10 and 11. The effects of mean flow are clearly evident, causing the attenuation to be greatly subdued. Whereas there is some variability in the attenuation spectra for the no-flow condition, the attenuation spectra for the four configurations tend to collapse as the mean flow is increased. Also, the frequency of peak attenuation shifts from 1200 Hz at Mach 0.0 to 1400 Hz at Mach 0.5.

VI. Concluding Remarks

This paper has explored the effects of variable-depth geometry on the resultant noise reduction achievable with an acoustic liner mounted in the NASA Langley Grazing Flow Impedance Tube (GFIT). Two variable-depth liners were tested in the GFIT, and were demonstrated to provide significant broadband noise reduction. The Two-Parameter impedance prediction model was used to estimate the impedance distribution over the surface of these two liners, and these impedance spectra were used as input for two propagation codes to predict the corresponding sound pressure level profiles over the length of the GFIT. The impedance prediction model and propagation codes were then used for investigation of a number of variable-depth liner configurations. A number of observations are provided based on the measured and predicted results:

1. At Mach 0.0, significant attenuation is observed over a frequency range of at least one octave with the variable-depth liners used in this study. This attenuation is reduced as the Mach number is increased.

2. Liner orientation (maximum depth at LE or TE) has a strong effect on the SPL profile over the length of the liner, but the effect on the total attenuation is less pronounced.

3. SPL profiles predicted with two propagation codes (CHE and CDL) exhibit similar trends to those measured in the GFIT. This comparison is most favorable when the effects of mean flow are included, and at frequencies for which the attenuation is not large. At Mach 0.0, there is significant attenuation for frequencies near resonance, and the comparison of predicted and measured SPL profiles is slightly less favorable. Overall, the SPL profiles predicted with each of these codes are sufficiently similar to the measured profiles to support the usage of the impedance prediction model and either propagation code for evaluation of proposed variable-depth liner configurations.

4. The axial extent of attenuation for an individual frequency continues well beyond the location where the liner depth is optimally tuned to the quarter-wavelength of that frequency.

5. The SPL profile is significantly affected by the way in which variable-depth segments are distributed over the length of the liner. However, the total amount of attenuation is relatively unaffected.

Further development of an impedance prediction method specifically designed for this application is needed. Also, further evaluation of the effects of impedance discontinuities on the propagation codes used in this study is warranted. These issues are expected to be addressed in future studies.

Acknowledgments

The authors would like to express appreciation to Martha Brown and Carol Harrison of NASA Langley Research Center for assistance in the GFIT testing. The Advanced Air Transport Technology Project of NASA's Advanced Air Vehicles Program funded this work.

References

[1]Jones, M. G., Watson, W. R., Nark, D. M., and Howerton, B. M., "Evaluation of a Variable-Impedance Ceramic Matrix Composite Acoustic Liner," AIAA Paper 2014-3352, June 2014.

[2]Motsinger, R. E. and Kraft, R. E., "Design and Performance of Duct Acoustic Treatment: Aeroacoustics of Flight Vehicles; Chapter 14, Vol. 2: Noise Control," NASA RP 1258, August 1991.

[3]Parrott, T. L. and Jones, M. G., "Assessment of NASA's Aircraft Noise Prediction Capability, Chapter 6: Uncertainty in Acoustic Liner Impedance Measurement and Prediction," NASA TP 2012-215653, July 2012.

[4]Nark, D. M., "Assessment of Radiated Fan Noise Prediction Capabilities using Static Engine Test Data," AIAA Paper 2011-2807, June 2011.

[5]Watson, W. R. and Nark, D. M., "Assessment of NASA's Aircraft Noise Prediction Capability, Chapter 6: Assessment of Acoustic Propagation and Radiation Codes for Locally Reacting Liners in Flow Ducts," NASA TP 2012-215653, July 2012.

[6]Bendat, J. S. and Piersol, A. G., *Random Data: Analysis and Measurement Procedures*, Wiley-Interscience, 1971.

[7]Wilcox, D. C., *Basic Fluid Mechanics*, DCW Industries, 1998.

[8]L. Green, J. and Duwez, P., "Fluid Flow Through Porous Materials," *Journal of Applied Mechanics*, 1951, pp. 39–45.

[9]Melling, T. H., "The Acoustic Impedance of Perforates at Medium and High Sound Pressure Levels," *Journal of Sound and Vibration*, Vol. 29, No. 1, 1973, pp. 1–65.

[10]Heidelberg, L. J., Rice, E. J., and Homyak, L., "Experimental Evaluation of a Spinning-Mode Acoustic-Treatment Design Concept for Aircraft Inlets," NASA TP 1613, April 1980.

[11]Watson, W. R., Jones, M. G., and Parrott, T. L., "Validation of an Impedance Eduction Method in Flow," *AIAA Journal*, Vol. 37, No. 7, July 1999, pp. 818–824.

[12]Nark, D. M. and Jones, M. G., "Broadband Liner Optimization for the Source Diagnostic Test Fan," AIAA Paper 2012-2195, June 2012.

[13]Parrott, T. L., Abrahamson, A. L., and Jones, M. G., "Measured and Calculated Acoustic Attenuation Rates of Tuned Resonator Arrays for Two Surface Impedance Distribution Models with Flow," NASA TP 1613, January 1988.